The Journal of Physical Chemistry A

 VOLUME 102, NUMBER 22, MAY 28, 1998

ARTICLES

Vibrational Energy Transfer in Methane Excited to $2\nu_3$ in CH_4-N_2/O_2 Mixtures from Laser-Induced Fluorescence Measurements

L. Doyennette,*,† F. Menard-Bourcin, J. Menard, C. Boursier, and C. Camy-Peyret

Laboratoire de Physique Moléculaire et Applications,‡ CNRS, Université Pierre et Marie Curie, Tour 13, Bte 76, 4 Place Jussieu, 75252 Paris Cedex 05, France

Received: January 6, 1998; In Final Form: March 11, 1998

Vibrational energy transfer processes in CH_4-N_2/O_2 mixtures have been investigated by using the laser-induced fluorescence method. Methane molecules were excited to the $2\nu_3$ vibrational state by an optical parametric oscillator pumped by a Nd:YAG laser, and hot fluorescence from combination and overtone states was monitored for both infrared active modes: ν_3 near 3.3 μm, and ν_4 near 7.5 μm. The ν_3 fluorescence exhibits a decay fitted by two exponential functions of time, while the ν_4 fluorescence shows an increase followed by a decay. The time dependence of the observed fluorescence signals was used to derive rate constants which were found to vary linearly as a function of the molar fraction of CH_4 in the gas mixtures. A numerical kinetic model, in which the populations of vibrational states with given numbers of stretching and bending excitation quanta are assumed to be in instantaneous equilibrium, has allowed to reproduce the time evolution of fluorescence intensities and to determine rate coefficients for intermode and V−V transfer processes occurring upon CH_4-CH_4 and CH_4-N_2/O_2 collisions.

I. Introduction

Methane is a minor atmospheric constituent whose concentration is relatively uniform in the troposphere and the low stratosphere (volume mixing ratio approximately equal to 1.7 ppm). Therefore, using laser techniques, the CH_4 molecule could possibly be used as a probe of its environment: it could be excited to the $2\nu_3$ vibrational state, in the atmospheric window at 1.6−1.7 μm where lines of the $2\nu_3$ band are easily recognized in atmospheric solar spectra,[1] and information on local atmospheric pressure and temperature could be deduced from the analysis of the laser-induced fluorescence emitted by the excited gas. Such analysis, however, needs a thorough understanding of the rovibrational relaxation of CH_4 upon collisions with the main atmospheric constituents.

Most of the kinetic information concerning vibrational energy transfer rates in methane has been provided by Moore et al. using the laser-induced fluorescence method.[2−7] Other works on V−T,R and V−V processes involving the lowest vibrational states, up to ν_3, have also been performed by using an optoacoustic method[8,9] or a time-resolved Raman scattering technique.[10] More recently, state-to-state rotational energy transfer measurements have been performed in the ground and $\nu_3 + \nu_4$ excited levels by Klassen et al.[11] using a time-resolved double resonance technique. But no work has yet been performed on the relaxation of $CH_4(2\nu_3)$ by N_2 and O_2, the two most important atmospheric constituents. The present work is a first contribution to this study. Methane has been excited to the $2\nu_3(F_2)$ vibrational state by an optical parametric oscillator pumped by a Nd:YAG laser, and hot fluorescence from combination and overtone states was monitored for both infrared active modes: ν_3 ($\Delta v_3 = -1$ bands) around 3.3 μm, and ν_4

† Fax: 33 1 44 27 70 33. E-mail: doyen@ccr.jussieu.fr.
‡ Laboratoire associé aux Universités P. et M. Curie et Paris-Sud.

S1089-5639(98)00646-X CCC: $15.00
Published on Web 05/06/1998

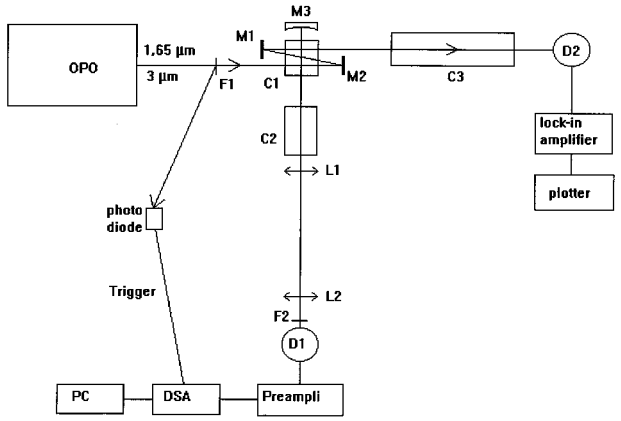

M1 et M2: plane mirrors
M3: spherical mirror
C1: fluorescence cell
C2, C3: absorption cells
F1, F2: filters
D1: InSb or HgCdTe detector
D2: pyroelectric detector
DSA: digital signal analyzer

Figure 1. Experimental setup used to detect the laser-induced fluorescence emitted at the ν_3 and ν_4 frequencies by CH_4 molecules excited to the $2\nu_3(F_2)$ state by an OPO.

($\Delta v_4 = -1$ bands) around 7.5 μm. Transfer rate constants were measured as a function of the molar fraction of CH_4 in CH_4-N_2/O_2 mixtures. Finally, a numerical model based on a kinetic analysis of the vibrational relaxation has been set up, allowing to reproduce the time evolution observed for the relaxation of the fluorescence and to determine the rate coefficients for various relaxation processes.

II. Experimental Section

A powerful tunable IR laser system was used to excite overtone levels of the asymmetric stretching vibration of methane. A Continuum Model Mirage 3000 optical parametric oscillator (OPO) is pumped by a Continuum Model Powerlite 7010 Nd:YAG laser. The Nd:YAG laser uses an oscillator/amplifier configuration; it is injection-seeded by a single-mode CW diode laser and produces output at the fundamental 1064 nm and harmonic 532 nm wavelength with 10 Hz pulse repetition rate. The output consists of single longitudinal mode (SLM) pulses about 7 ns in duration. The Mirage 3000 consists of an optical parametric master oscillator, operated in the near-infrared, followed by two successive parametric converter stages. The master oscillator pumped by the 532 nm output of the Nd:YAG laser is actively stabilized for SLM operation and controls the spectral performance while the parametric converters which consist of two phase-matched KTP crystals oriented in a counter-rotating geometry maximize the energy attainable in the mid-infrared. The first converter, pumped at 532 nm, amplifies the signal wave from the oscillator and produces an idler wave covering the spectral range 1.45−2.12 μm. Then by injecting this idler wave into the second converter, pumped at 1064 nm, amplification of this wave which becomes the new signal wave and generation of a new idler wave in the 2.12−4 μm range occur, thus producing tunable emission from 1.45 to 4 μm with 0.02 cm^{-1} line width. This system allowed excitation of well-isolated lines or groups of lines of the overtone $2\nu_3$ band of methane.

The excitation of the overtone $2\nu_3$ was performed by tuning the OPO signal wavelength to coincide with different $2\nu_3$ band lines, mostly the Q(6) line (1665.95 nm) of the Q branch and the R(3) line (1656.55 nm) of the R branch.[12] The fluorescence

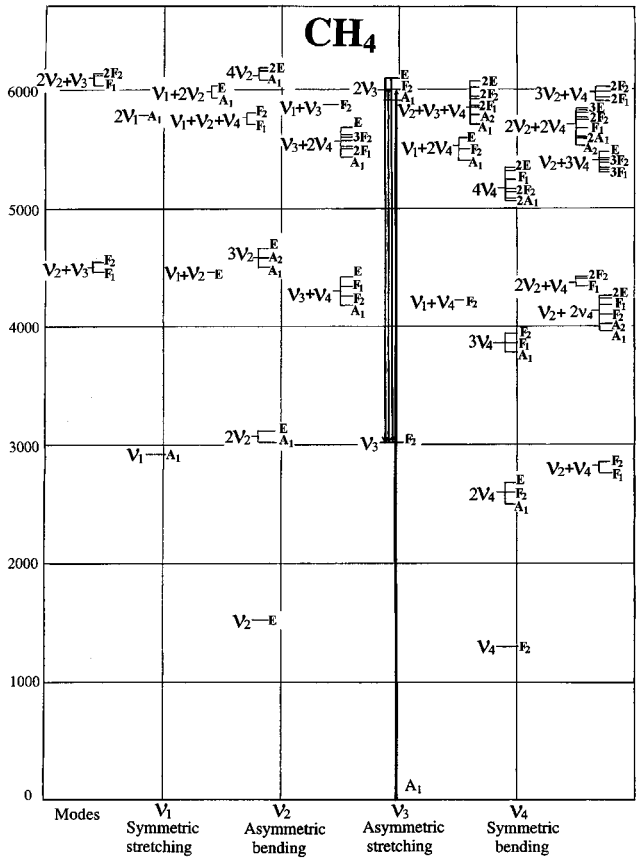

Figure 2. Vibrational levels of methane up to the states of the tetradecad. The vibrational subcomponents are shown for each state (60 components for the 14 states of the tetradecad).

experimental setup is shown in Figure 1. The OPO idler wavelength was removed by a bandpass filter transmitting only the desired excitation wavelength. The beam was directed into the fluorescence cell (C1) filled with the sample mixture and was reflected back twice through this cell by means of the M1 and M2 mirrors. Then it was sent through a 60 cm long absorption cell (C3) containing methane at 100 Torr pressure, and its transmitted intensity was detected by a pyroelectric energy meter (D2). The signal from this detector, amplified by a lock-in amplifier, was recorded allowing continuous control of the excitation wavelength.

The fluorescence cell C1 was a cylindrical Pyrex cell, 5 cm long, 4 cm in diameter, equipped with fluorine windows. Two side windows also fitted by fluorine plates allowed collection of the fluorescence emitted perpendicular to the pumping beam. The fluorescence radiation was focused onto an infrared detector (D1) by an optical arrangement consisting of a 5 cm focal length fluorine lens (L1) and a 6 cm focal length lens (L2) which formed onto the detector an image of magnification $^1/_2$ from the center of the cell. A spherical mirror M3, 25 mm in diameter and 60 mm in radius of curvature, located to the rear of the sample cell, is used to reflect back to the detector the fluorescence radiation passing through the rear window. A gas filter cell (C2) containing 100 Torr of CH_4 was placed between the fluorescence cell and the CaF_2 lens to eliminate fluorescence on the fundamental bands.

In order to block the scattered laser radiation and to separate the ν_3 and ν_4 fluorescence emissions, two different filters (F2) have been used in our experiments: a filter (F2) centered near 3.3 μm was used for the hot ν_3 fluorescence which was detected by a InSb detector (77 K); and a filter centered near 7.5 μm was used for the hot ν_4 fluorescence which was detected by a

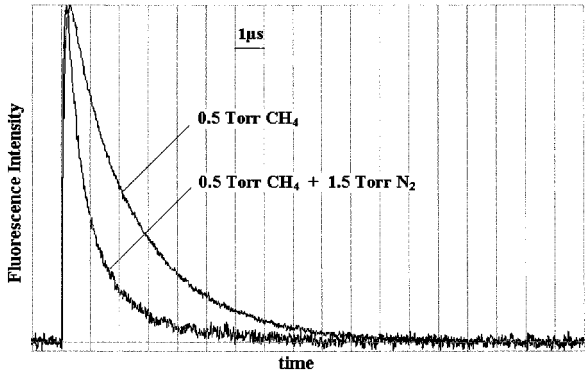

Figure 3. Signals showing the effect of N_2 addition on the decay vs time of the hot ν_3 fluorescence intensity following $2\nu_3(F_2)$ excitation of CH_4 molecules. CH_4 pressure is the same for both signals. The CH_4 relaxation is clearly enhanced by addition of N_2.

HgCdTe detector (77 K). The signal from the detector was preamplified with a bandwidth between 10 kHz and 20 MHz; then it was sampled, averaged, and recorded by a Tektronix DSA 610, the trigger pulse being derived from a photodiode ET2000 which received a part of the scattered laser signal. Finally, the averaged signals were transmitted for analysis to a microcomputer.

Methane, oxygen, and nitrogen with purity >99.995% were provided by Air Liquide. Gas pressures were measured with a 1.0 Torr capacitance manometer (MKS) and with a Bourdon gauge (Texas Instruments) for higher pressures.

III. Results

The CH_4 molecule has four vibrational modes: two bending vibrations ν_2 (asymmetric) and ν_4 (symmetric), and two stretching vibrations ν_1 (symmetric) and ν_3 (asymmetric). The first excited bending levels $\nu_2(E)$ and $\nu_4(F_2)$ are located at 1533 and 1311 cm^{-1}, respectively, and the stretching levels $\nu_1(A_1)$ and $\nu_3(F_2)$ at 2917 and 3019 cm^{-1}, respectively, approximately 2 times higher than the two former ones. Consequently, the vibrational energies of methane form clusters whose spacings are about 1500 cm^{-1}, and the vibrational states are gathered in polyads of interacting states which are successively, as shown in Figure 2, the (ν_2, ν_4) dyad, the (ν_1, ν_3, $2\nu_2$, $2\nu_4$, $\nu_2 + \nu_4$) pentad, an octad in the region around 4500 cm^{-1}, then a tetradecad around 6000 cm^{-1} involving the $2\nu_3$ state excited in our experiments. Strong interactions exist between the states of a given polyad, so that the spectroscopic analysis of any vibrational state needs to take into account simultaneously all the states of the polyad to which this state belongs.[13] This feature is important for the understanding of relaxation measurements: very fast energy transfer processes are expected to occur between the states of a polyad.

Furthermore, the $v_i > 1$ vibrational states are split into subcomponents of different symmetry. For instance, the $2\nu_3$ state is split into three components of vibrational symmetry A_1, E, and F_2. The dipolar transitions between vibrational states are determined by the following selection rules taking into account the symmetry of the states: all the transitions between vibrational states of symmetry A are forbidden, except the $A_1 \leftrightarrow F_2$ and $A_2 \leftrightarrow F_1$ transitions; all the transitions between vibrational states of symmetry E and F are allowed, except the $E \leftrightarrow E$ transition. Consequently, only the triply degenerate vibrations ν_3 and ν_4 are active in the infrared with dipolar transition moments equal to $\mu_3 = 0.0547$ and $\mu_4 = 0.0605$ D respectively.[14] Besides, only the F_2 subcomponent of $2\nu_3$ has electric dipole transitions with the $0(A_1)$ fundamental state, so

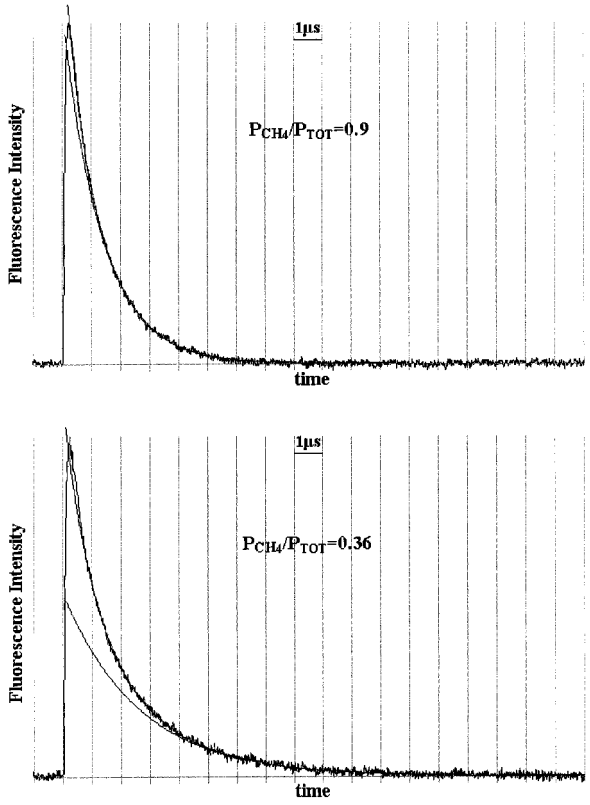

Figure 4. Time decay of the hot ν_3 fluorescence intensity following $2\nu_3(F_2)$ excitation of CH_4 molecules in two CH_4-N_2 mixtures. The total pressure is 1 Torr for the two mixtures, but the CH_4 molar fraction z is 0.9 and 0.36, respectively. The fit of the slow final part of the decay by a single-exponential function of time is given in solid line. It shows that the contribution of the fast part of the decay is much larger for the smallest molar fraction $z = 0.36$.

that, in our experiments, CH_4 molecules have been actually excited to rovibrational levels of the $2\nu_3(F_2)$ state corresponding to different lines of the $2\nu_3(F_2) \leftarrow 0(A_1)$ band. But the three vibrational subcomponents of $2\nu_3$ have electric dipole transitions with ν_3 producing the hot fluorescence $2\nu_3 \rightarrow \nu_3$ infrared emission.

All our measurements were performed using a CH_4 gas filter cell to eliminate the fundamental fluorescence. Emissions near $\nu_3 = 3.3$ μm and near $\nu_4 = 7.5$ μm were successively observed using appropriate detectors and filters. The relaxation of these emissions was studied by exciting CH_4 molecules at frequencies corresponding to different lines of the P, Q, and R branches of the $2\nu_3(F_2) \leftarrow 0(A_1)$ band; but no difference in the relaxation time was obtained with these different lines. However, most of our measurements were performed by using either the R(3) or Q(6) line because the largest intensities were obtained with these lines.

Relaxation measurements were carried out at room temperature in CH_4-N_2/O_2 gas mixtures with pressures in the 0.1−10 Torr range and the fluorescence signals were recorded for times in the 8−100 μs range. The collisional transfer processes investigated in our experiments are much more rapid than the radiative processes characterized by a lifetime of 20 ms for the fastest process and than the wall-deexcitation process (about 3 ms for 1 Torr of neat CH_4).

A. Fluorescence at the ν_3 Frequency. The fluorescence intensity near 3.3 μm was relatively strong and was detectable in our experimental conditions for CH_4 pressures as low as 10 mTorr. The intensity decreases versus time with decay rates in the 10^4-10^6 s^{-1} range for the pressures used in our

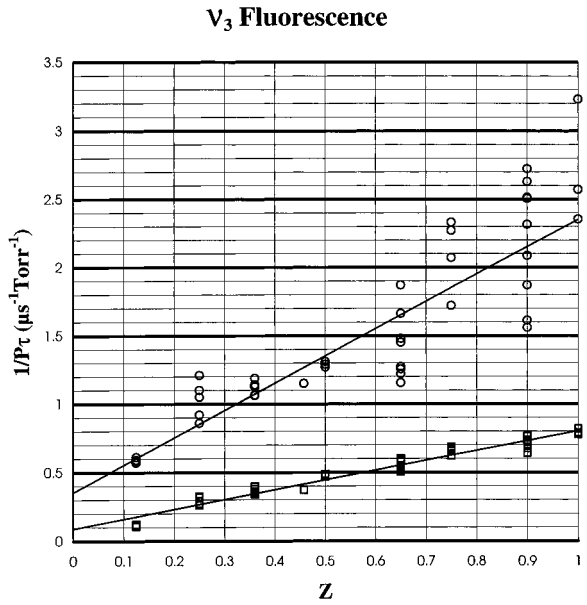

Figure 5. Molar fraction dependence of the two rate constants $1/P\tau_f$ and $1/P\tau_s$ measured in CH_4-N_2 mixtures. The linear best fits of the experimental values (○ and □) are given by the solid lines.

experiments. The addition of N_2 or O_2 results in an increase of the decay rate. This is illustrated in Figure 3 showing two fluorescence signals obtained with a same CH_4 pressure of 0.5 Torr, but the first one in pure CH_4 and the other one in a 2 Torr of CH_4-N_2 mixture. This second signal exhibits a much larger decay rate than the first one. Such signals are well fitted by a weighted sum of two exponential functions of time from which two rate constants (a fast and a slow one) $1/P\tau_f$ and $1/P\tau_s$ can be deduced. These rate constants have been determined as a function of the molar fraction z of CH_4 in CH_4-M mixtures with $M = N_2$ or O_2. The weight of the fastest exponential function from which the larger rate constant $1/P\tau_f$ is deduced was found to be very small for z around 1 and increasing as the molar fraction z was decreasing. Consequently, values of $1/P\tau_f$ have been determined with a better accuracy for small values of z than for $z \sim 1$. On the contrary, the determination of $1/P\tau_s$ was more accurate for $z \sim 1$ than for the small values of z where the contribution of the fast exponential function becomes preponderant. This is illustrated in Figure 4 by two signals obtained with CH_4-N_2 mixtures: in both cases, the total gas pressure is 1 Torr, but the CH_4 partial pressures are different, the molar fraction z being 0.9 and 0.36, respectively. For $z = 0.9$, the signal is rather well fitted by a single-exponential function of time as shown by the calculated signal (in solid line in the figure), except in the first microsecond during which a slight difference is observed between the calculated signal and the experimental one. This difference increases while z decreases, as can be seen in Figure 4, during the first three microseconds of the signal corresponding to $z = 0.36$. The difference between the observed signal and the calculated curve obtained by fitting the long time part of the fluorescence signal with a single-exponential function is larger just after the excitation pulse.

The results obtained for $1/P\tau_f$ and $1/P\tau_s$ with CH_4-N_2 mixtures have been plotted versus z in Figure 5. Considering the relatively large uncertainties in the determination of these rate constants, no significant difference was found between these results and those obtained with CH_4-O_2 mixtures. One can see in Figure 5 that these rate constants vary linearly as a function of z. Consequently, they can be written as:

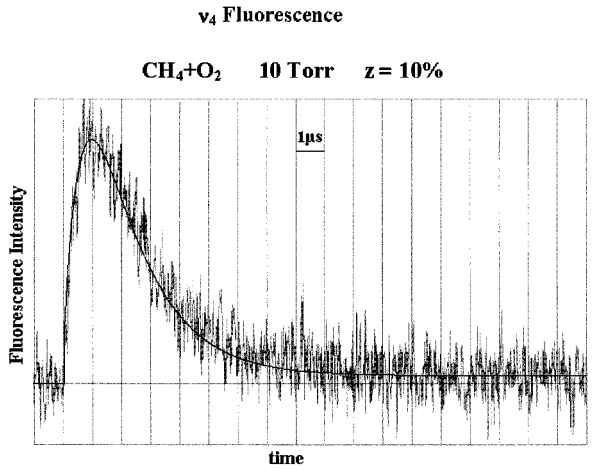

Figure 6. Time evolution of the hot ν_4 fluorescence intensity following the $2\nu_3(F_2)$ excitation of CH_4 molecules in a CH_4-O_2 mixture. The fit of the signal by a difference of two exponentials as a function of time is given by the solid line.

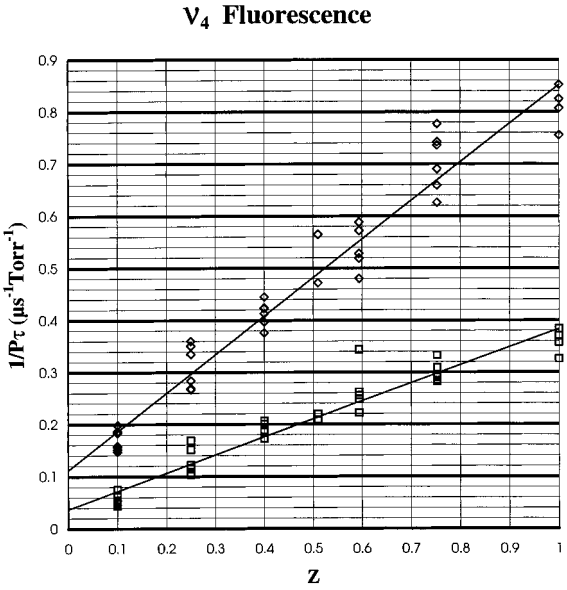

Figure 7. Molar fraction dependence of the two rate constants corresponding to the time increase and decrease of the hot ν_4 fluorescence intensity. The linear best fits of the experimental values (◇ and □) are given by the solid lines.

$$1/P\tau = (1/P\tau)_{CH_4-CH_4} z + (1/P\tau)_{CH_4-M}(1 - z)$$

$(1/P\tau)_{CH_4-CH_4}$ and $(1/P\tau)_{CH_4-M}$ being the rate constants corresponding to CH_4-CH_4 and CH_4-M collisions with $M = N_2$ or O_2.

The following results have been obtained:

1. For the slow decay, the intercepts of the linear best fit of $1/P\tau_s$ at $z = 1$ and $z = 0$ yield, in s^{-1} $Torr^{-1}$, $(1/P\tau_s)_{CH_4-CH_4} = (8.1 \pm 0.9) \times 10^5$ and $(1/P\tau_s)_{CH_4-M} = (1.0 \pm 0.15) \times 10^5$, respectively. Note that the value of $(1/P\tau_s)_{CH_4-CH_4}$ is equal to that previously found by Hess et al.[7]

2. In the same way, for the fast decay, the linear best fit of $1/P\tau_f$ yields, in s^{-1} $Torr^{-1}$, $(1/P\tau_f)_{CH_4-CH_4} = (2.45 \pm 0.60) \times 10^6$ at $z = 1$, and $(1/P\tau_f)_{CH_4-M} = (3.5 \pm 0.8) \times 10^5$ at $z = 0$.

B. Fluorescence at the ν_4 Frequency. The fluorescence intensity detected near $\nu_4 = 7.5$ μm is much smaller than that detected at the ν_3 frequency. A typical fluorescence signal obtained with a 10 Torr CH_4-O_2 mixture and a CH_4 molar fraction z equal to 10% is given in Figure 6. The signal exhibits

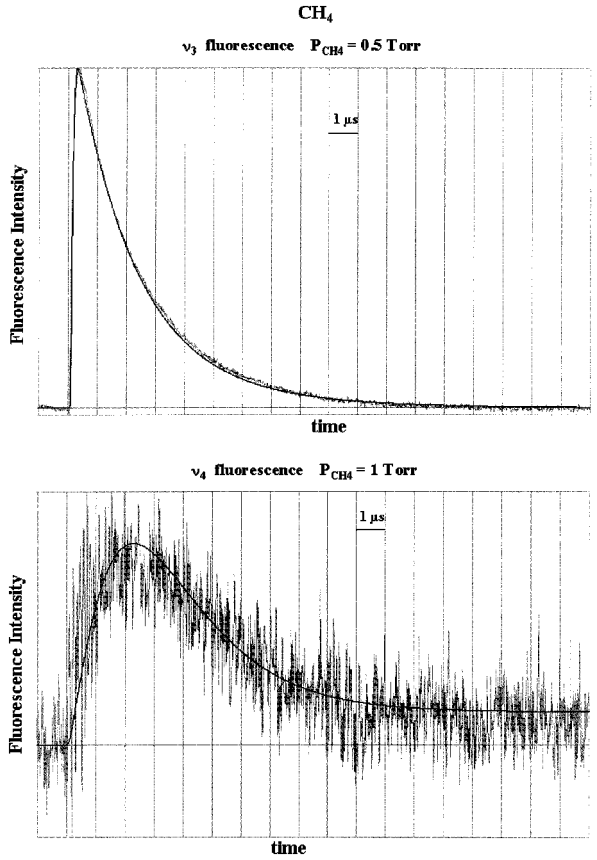

Figure 8. Hot ν_3 and ν_4 fluorescence signals simulated by the kinetic model using the rate coefficients values indicated in text superimposed on the corresponding experimental signals obtained in pure CH_4.

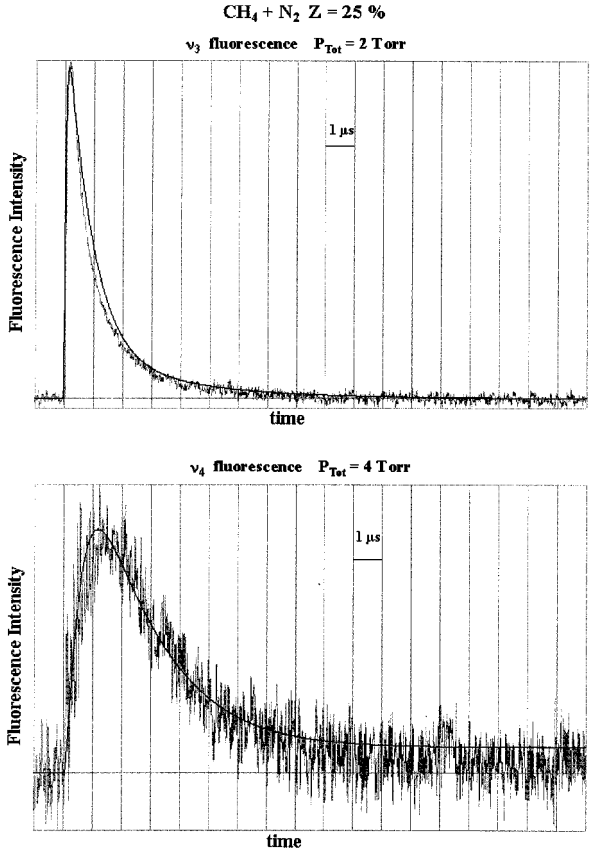

Figure 9. Same as Figure 8 for a $CH_4 + N_2$ mixture with a CH_4 molar fraction of 0.25.

first a fast increase followed by a slower decay. This proves that fast vibrational energy transfer occurs from stretching to bending modes. The observed time evolution is well fitted by a difference of two exponentials (solid line in the figure) from which two rate constants can be deduced. Measured as a function of the molar fraction z, these two rate constants vary linearly versus z as shown in Figure 7. The rate constants corresponding to the increase of the ν_4 fluorescence were found to be equal to $(8.5 \pm 0.9) \times 10^5$ s^{-1} Torr^{-1} at $z = 1$, and $(1.1 \pm 0.15) \times 10^5$ s^{-1} Torr^{-1} at $z = 0$, values very similar to those corresponding to the slow decay of the ν_3 fluorescence in the same mixture. The rate constants corresponding to the decay of the ν_4 fluorescence were found to be equal to $(3.8 \pm 0.6) \times 10^5$ s^{-1} Torr^{-1} at $z = 1$, and $(4.0 \pm 0.8) \times 10^4$ s^{-1} Torr^{-1} at $z = 0$. These relatively slow rates may be primarily considered as rates of depletion of the pentad. Let us recall that the pentad levels contributes to the hot ν_4 fluorescence whereas the hot ν_3 fluorescence does not include the pentad levels.

No significant difference was found between the results obtained with CH_4-N_2 and CH_4-O_2 mixtures.

IV. Kinetic Model

Following laser excitation into rovibrational levels of $2\nu_3(F_2)$, a fast rotational equilibration occurs in some 10^7 s^{-1} Torr^{-1} [11,15] among the levels of the excited vibrational state. Then the vibrational energy spills over from $2\nu_3(F_2)$ to the two other vibrational subcomponents $2\nu_3(A_1)$ and $2\nu_3(E)$ at a rate certainly much larger than those measured for the decay of the ν_3 and ν_4 fluorescence intensity. Indeed, in order to determine the corresponding rate constants, fluorescence measurements have been performed by using two narrow filters centered on the Q-branch of the $2\nu_3(A_1) \rightarrow \nu_3(F_2)$ and $2\nu_3(E) \rightarrow \nu_3(F_2)$ bands, respectively. One could have expected to observe first a rise vs time of the fluorescence intensity due to the $2\nu_3(F_2) \leftrightarrow 2\nu_3(A_1)$ and $2\nu_3(F_2) \leftrightarrow 2\nu_3(E)$ transfer processes. But only a decay was observed, at least down to the lowest CH_4 pressure of 0.5 Torr for which a fluorescence signal was still detectable. This demonstrates that the populations of the subcomponents of the $2\nu_3$ vibrational state are very rapidly equilibrated, and can be considered in instantaneous equilibrium for the time × pressure scales used in the present relaxation measurements of the hot ν_3 and ν_4 fluorescence. This will also be assumed for all the other vibrational states so that no discrimination will be made in the following model between the vibrational subcomponents of a given vibrational level.

Then we have to take into account 30 vibrational levels in the kinetic model: 14 for the tetradecad, 8 for the octad, 5 for the pentad, 2 for the dyad, plus one for the fundamental level. In principle, each fluorescence signal should be analyzed as a sum of several exponentials, the number of which being the number of levels (or group of levels) involved in the relaxation. However, for the empirical analysis of the fluorescence signals observed in our experiments, it was not possible to fit the time dependence of the signals with more than two exponentials. The rates retrieved from the ν_3 and ν_4 fluorescence signals, as discussed above, are then related to the individual contribution of many energy transfer processes coupling the vibrational states. In order to get a better understanding of the relaxation pathway, simplifying hypotheses are then necessary. Considering the strong interactions existing between the vibrational states of a polyad, we shall assume that vibrational levels with given numbers of stretching and bending excitation quanta have their populations in instantaneous equilibrium and form a pseudo-level. For example, the $2\nu_3$, $\nu_1 + \nu_3$, and $2\nu_1$ levels form a

pseudo-level called $2\nu_s$ (s for stretching); in the same way the $\nu_1 + 2\nu_4$, $\nu_1 + 2\nu_2$, $\nu_1 + \nu_2 + \nu_4$, $\nu_3 + 2\nu_4$, $\nu_3 + 2\nu_2$, and $\nu_3 + \nu_2 + \nu_4$ levels form the $\nu_s + 2\nu_b$ (b for bending) pseudo-level. This hypothesis is justified by the very fast equilibration observed by Hess et al.[7] between the two stretching modes up to the octad levels ($\nu_1 + \nu_4$ and $\nu_3 + \nu_4$) or between the two bending modes.

Finally, the set of levels taken into account in our kinetic model consists of the ground-state plus 8 pseudo-levels: $2\nu_s$, $\nu_s + 2\nu_b$ and $4\nu_b$ for the tetradecad, $\nu_s + \nu_b$ and $3\nu_b$ for the octad, ν_s and $2\nu_b$ for the pentad, and ν_b for the dyad.

Let us consider now the various energy transfer processes relaxing methane after excitation in the $2\nu_s$ pseudo-level:

1. *Intermode transfer processes* converting one stretching quantum in two bending quanta (let us recall that $\nu_s \sim 2\nu_b$) and so connecting pseudo-levels within each polyad:

tetradecad:

$$CH_4(2\nu_s) + CH_4\ (\text{or M}) \leftrightarrow CH_4(\nu_s{+}2\nu_b) + CH_4\ (\text{or M}) \quad (1)$$

$$CH_4(\nu_s{+}2\nu_b) + CH_4\ (\text{or M}) \leftrightarrow CH_4(4\nu_b) + CH_4\ (\text{or M}) \quad (2)$$

octad:

$$CH_4(\nu_s{+}\nu_b) + CH_4\ (\text{or M}) \leftrightarrow CH_4(3\nu_b) + CH_4\ (\text{or M}) \quad (3)$$

pentad:

$$CH_4(\nu_s) + CH_4\ (\text{or M}) \leftrightarrow CH_4(2\nu_b) + CH_4\ (\text{or M}) \quad (4)$$

where M is a foreign gas (O_2 or N_2).

2. *Near-resonant V−V transfer processes* with exchange of one stretching quantum or one bending quantum between two CH_4 molecules:

coupling the tetradecad to the pentad:

$$CH_4(2\nu_s) + CH_4(0) \leftrightarrow CH_4(\nu_s) + CH_4\ (\nu_s) \quad (5)$$

$$CH_4(\nu_s{+}2\nu_b) + CH_4(0) \leftrightarrow CH_4(\nu_s) + CH_4\ (2\nu_b) \quad (6)$$

coupling the tetradecad to the octad and the dyad:

$$CH_4(\nu_s{+}2\nu_b) + CH_4(0) \leftrightarrow CH_4(\nu_s{+}\nu_b) + CH_4\ (\nu_b) \quad (7)$$

$$CH_4(4\nu_b) + CH_4(0) \leftrightarrow CH_4(3\nu_b) + CH_4\ (\nu_b) \quad (8)$$

coupling the octad to the pentad and the dyad:

$$CH_4(\nu_s{+}\nu_b) + CH_4(0) \leftrightarrow CH_4(\nu_s) + CH_4\ (\nu_b) \quad (9)$$

$$CH_4(3\nu_b) + CH_4(0) \leftrightarrow CH_4(2\nu_b) + CH_4\ (\nu_b) \quad (10)$$

coupling the pentad to the dyad:

$$CH_4(2\nu_b) + CH_4(0) \leftrightarrow CH_4(\nu_b) + CH_4\ (\nu_b) \quad (11)$$

The V−T, R relaxation processes, occurring on a much longer time scale (~ 700[3] or 850[4] s^{-1} $Torr^{-1}$ for neat CH_4, 64 and 164 s^{-1} $Torr^{-1}$[13] for CH_4-N_2 and CH_4-O_2 mixtures, respectively) have been neglected in our relaxation scheme.

Finally, the 9 levels or pseudo-levels are connected by 11 processes. The following assumptions have been made for the rate coefficients:

1. All intermode transfer processes have the same rate coefficient, $k^i_{CH_4-CH_4}$ for self-collisions and $k^i_{CH_4-M}$ for collisions with a foreign gas.

2. The rate coefficients of near-resonant V−V transfer processes are related by a scaling factor appropriate to first-order perturbation theory for harmonic oscillators. For example, the rate coefficient of process (11) is 2 times larger than the rate coefficient of process (9). The rate coefficients of processes involving transitions between levels $\upsilon_s = 0$ and $\upsilon_s = 1$ or transitions between $\upsilon_b = 0$ and $\upsilon_b = 1$ are noted k^s_{V-V} and k^b_{V-V}, respectively.

The set of differential equations describing the time evolution of the populations of the 9 vibrational levels or pseudo-levels is numerically solved using a Runge−Kutta method. The laser excitation has been modeled by adding to the set of differential equations a time-dependent term accounting for the increase in population of the $2\nu_s$ pseudo-level and for the corresponding decrease of the ground-state population. This term corresponds to the experimental time evolution of the pumping pulse. From the time evolution of the pseudo-levels populations, fluorescence signals are simulated and can be compared to experimental signals. The rate coefficients $k^i_{CH_4-CH_4}$, $k^i_{CH_4-M}$, k^s_{V-V}, and k^b_{V-V} were varied till the best agreement was obtained between simulated and experimental signals leading to the following values for the rate coefficients:

$$k^i_{CH_4-CH_4} = (7 \pm 2) \times 10^5\ s^{-1}\ Torr^{-1}$$

$$k^i_{CH_4-M} = (6 \pm 2) \times 10^5\ s^{-1}\ Torr^{-1}$$

$$k^s_{V-V} = (3 \pm 1) \times 10^5\ s^{-1}\ Torr^{-1}$$

$$k^b_{V-V} = (3 \pm 1) \times 10^5\ s^{-1}\ Torr^{-1}$$

Figures 8 and 9 present simulated signals superimposed on the corresponding experimental signals for neat CH_4 and a CH_4-N_2 mixture with a CH_4 molar fraction of 0.25, respectively. One can see the very good agreement obtained for neat CH_4 for the ν_3 fluorescence as well as for the ν_4 fluorescence. The agreement is not so good for the ν_3 fluorescence when the CH_4 molar fraction decreases probably because the assumption of instantaneous equilibrium between vibrational levels forming a pseudo-level is less valid when the molar fraction is small.

A better spectroscopic knowledge of interactions between the vibrational states in the tetradecad could allow a better gathering of these states into pseudo-levels and so could improve the kinetic model. However, the present kinetic model, although very simple, allows a reasonably global picture of the relaxation pathways in highly excited methane.

V. Conclusion

Our relaxation measurements using the laser-induced fluorescence technique have shown that the CH_4-N_2/O_2 collisions are very efficient for intermode transfer between states of the

CH_4 tetradecad. The ν_3 fluorescence was observed, as well as the ν_4 fluorescence which indicates that fast vibrational energy transfer exist from stretching to bending modes. Similar rate constants, within the experimental accuracy, were measured for CH_4-N_2 and CH_4-O_2 collisions. These collisions are involved in intermode transfers between interacting vibrational states. Such fast transfers are certainly related to rotational energy transfers which have a predominant effect on line pressure broadening. From this point of view, our results are consistent with line width measurements in the ν_3 region of methane showing close values for O_2 and N_2 broadening.[16,17]

Finally, a new kinetic model of the methane relaxation has allowed the determination of rate coefficients for intermode and V−V transfer processes occurring upon CH_4-CH_4 and CH_4-N_2/O_2 collisions.

The observed fluorescence signals represent a global emission in all the $\Delta v_3 = -1$ and $\Delta v_4 = -1$ bands, except the fundamental ones, and the time evolution of the fluorescence is related to the populations of all the emitting vibrational levels. A more detailed understanding of the relaxation pathways would need monitoring of the populations of selected vibrational levels. This will be the purpose of future time-resolved IR−IR double resonance experiments.

References and Notes

(1) Delbouille, L.; Rolland, G.; Brault, J.; Testerman, L. *Photometric atlas of the solar spectrum from 1850 to 10, 000 cm*$^{-1}$; Inst. d'Astrophys. de Liège, Kitt Peak National Observatory, 1982.
(2) Yardley, J. T.; Moore, C. B. *J. Chem. Phys.* **1966**, *45*, 1066.
(3) Yardley, J. T.; Moore, C. B. *J. Chem. Phys.* **1968**, *48*, 14.
(4) Yardley, J. T.; Moore, C. B. *J. Chem. Phys.* **1968**, *49*, 1111.
(5) Yardley, J. T.; Fertig, M. N.; Moore, C. B. *J. Chem. Phys.* **1970**, *52*, 1450.
(6) Hess, P.; Moore, C. B. *J. Chem. Phys.* **1976**, *65*, 2339.
(7) Hess, P.; Kung, A. H.; Moore, C. B. *J. Chem. Phys.* **1980**, *72*, 5525.
(8) Avramides, E.; Hunter, T. F. *Chem. Phys.* **1981**, *57*, 441.
(9) Perrin, M. Y.; Jolicard, G. *Chem. Phys.* **1984**, *91*, 341.
(10) Kosterev, A. A.; Malinovsky, A. L.; Ryabov, E. A. *Chem. Phys. Lett.* **1992**, *199*, 349.
(11) Klassen, J. J.; Coy, S. L.; Steinfeld, J. I. *J. Chem. Phys.* **1994**, *101*, 10533.
(12) Margolis, J. S. *Appl. Opt.* **1988**, *27*, 4038 and references therein.
(13) Champion, J. P.; Loëte, M.; Pierre, G. *Spectroscopy of the Earth's Atmosphere and Interstellar Medium*; Rao K. N., Weber A., Eds.; Spherical Top Spectra; Academic Press Inc.: Columbus, 1992; pp 339−422.
(14) Fox, K.; Person, W. B. *J. Chem. Phys.* **1976**, *64*, 5218.
(15) Millot, G.; Lavorel, B.; Steinfeld, J. I. *J. Chem. Phys.* **1991**, *95*, 7938.
(16) Pine, A. S. *J. Chem. Phys.* **1992**, *97*, 773.
(17) Benner, D. C.; Devi, V. M.; Smith, M. A. H.; Rinsland, C. P. *J. Quant. Spectrosc. Radiat. Transfer* **1993**, *50*, 65.